

Solar axions cannot explain the XENON1T excess

Luca Di Luzio,^{1,*} Marco Fedele,^{2,†} Maurizio Giannotti,^{3,‡} Federico Mescia,^{2,§} and Enrico Nardi^{4,¶}

¹*Deutsches Elektronen-Synchrotron DESY, Notkestraße 85, D-22607 Hamburg, Germany*

²*Dept. de Física Quàntica i Astrofísica, Institut de Ciències del Cosmos (ICCUB),*

Universitat de Barcelona, Martí i Franquès 1, E-08028 Barcelona, Spain

³*Physical Sciences, Barry University, 11300 NE 2nd Ave., Miami Shores, FL 33161, USA*

⁴*INFN, Laboratori Nazionali di Frascati, C.P. 13, 100044 Frascati, Italy*

We argue that the interpretation in terms of solar axions of the recent XENON1T excess is not tenable when confronted with astrophysical observations of stellar evolution. We discuss the reasons why the emission of a flux of solar axions sufficiently intense to explain the anomalous data would radically alter the distribution of certain type of stars in the color-magnitude diagram in first place, and would also clash with a certain number of other astrophysical observables. Quantitatively, the significance of the discrepancy ranges from 3.3σ for the rate of period change of pulsating white dwarfs, and exceeds 19σ for the R -parameter and for $M_{I,\text{TRGB}}$.

Introduction. The XENON1T collaboration [1] has reported an excess in low-energy electronic recoil data below 7 keV and peaking around 2-3 keV. The collaboration cautions that the excess could be due to an unaccounted background from β decays due to a trace amount of tritium, but they also explore the possibility that the signal is due to different types of new physics. The most intriguing interpretation, which also provides the best fit to the data, is given in terms of solar axions, favoured over the background-only hypothesis at the 3.5σ level.

Three production mechanisms contribute to the solar axion flux: *i*) Atomic recombination and deexcitation, Bremsstrahlung, and Compton (ABC) interactions [2] that are controlled by the axion-electron coupling g_{ae} , *ii*) Primakoff conversion of photons into axions [3] induced by the axion-photon coupling $g_{a\gamma}$, *iii*) axion emission in the M1 nuclear transition of ^{57}Fe [4] that produces mono-energetic 14.4 keV axions, and is controlled by and effective axion-nucleon coupling g_{an}^{eff} . Since this last process cannot play any role in producing events below 10 keV, we will not include in our analysis astrophysical observables sensitive to g_{an}^{eff} . Conversely, axions produced through *i*) and *ii*) feature a wide spectrum peaking around a few keV. The production rates are independent of the axion mass for $m_a \lesssim 100$ eV. As regards detection, electron recoils occur via the axio-electric effect which is controlled by g_{ae} . Because of this, and because the location of the peak around 2-3 keV corresponds roughly to the maximum of the axion energy spectrum for the ABC processes, the Primakoff and ^{57}Fe components are both allowed to be absent as long as there is a nonzero ABC component. This selects g_{ae} as the crucial coupling to attempt to explain the data in terms of the QCD axion [5–8].¹ Taken at face value the strength of the XENON1T

excess requires $g_{ae} \gtrsim 10^{-12}$, corresponding to an axion decay constant $f_a \lesssim 10^8$ GeV, and in turn to an axion mass $m_a \gtrsim 0.06$ eV. However, astrophysical considerations indicate that such a large value of g_{ae} is not tenable, as stellar evolution would be drastically affected by the exceedingly large energy losses via axion emission. The strategy that we will follow consists in assuming that g_{ae} and $g_{a\gamma}$ lie in the 90% C.L. regions resulting from the XENON1T fit [1]. We will then estimate the effects of extra energy losses on a set of astrophysical observables related to Red Giants Branch (RGB) and Horizontal Branch (HB) stars, and to White Dwarfs (WDs).

Astrophysical observables and axion couplings.

The axion interactions with photons and electrons read

$$\mathcal{L}_{\text{int}} = \frac{1}{4} g_{a\gamma} a F_{\mu\nu} \tilde{F}^{\mu\nu} + g_{ae} \frac{\partial_\mu a}{2m_e} \bar{e} \gamma^\mu \gamma_5 e, \quad (1)$$

where the couplings can be related to model-dependent dimensionless coefficients as $g_{a\gamma} = \frac{\alpha}{2\pi} \frac{C_{a\gamma}}{f_a}$ and $g_{ae} = C_{ae} \frac{m_e}{f_a}$. In benchmark axion models $C_{a\gamma}$ and C_{ae} are typically of $\mathcal{O}(1)$, although strong enhancements/suppressions are possible in specific cases [9–13]. In the following, we will adopt the notation $g_{\gamma 10} \equiv g_{a\gamma} \times (10^{10} \text{ GeV})$ and $g_{e 13} \equiv g_{ae} \times 10^{13}$. Axions with couplings as large as $g_{e 13} \sim 10$, $g_{\gamma 10} \sim 1$ would be abundantly produced in several types of stars without being trapped, and thus would efficiently drain energy from the star cores

Astrophysical considerations have been systematically used to place severe bounds on light, weakly interacting particles, such as neutrinos and axions [14]. Noticeably, a set of anomalous observations have recently led to speculations that new physics is at play [13, 15, 16], and the axion case appears especially compelling [17, 18]. The most effective observables to constrain g_{ae} and $g_{a\gamma}$ are described below.

- *Tip of RGB stars in globular cluster.* We denote by $M_{I,\text{TRGB}}$ the luminosity of the tip of the RGB in globular clusters. RG stars are characterized by a He core and

¹ Our results apply also to explanations based on generic axion-like particles, for which there is no theoretical relation between m_a and the coupling strengths, and that are unrelated to the strong CP problem.

a burning H shell. During the RGB evolution, the ashes from the burning shell increase the He core mass, while the star luminosity (determined by equilibrium at the surface of the He core between thermal pressure supporting the non-degenerate envelope against the gravity pull from the core) keeps growing. The process continues until the core reaches sufficiently large temperatures and densities ($T \sim 10^8$ K, $\rho = 10^6$ g cm $^{-3}$) to ignite He, an event known as the He-flash. At this stage the star has reached its maximum luminosity $M_{I,\text{TRGB}}$, after which it shrinks and moves to the HB. If an additional core-cooling mechanism were at play, He ignition would be delayed, the core would accrete a larger mass, and the star would reach higher luminosities. Therefore, measurements of $M_{I,\text{TRGB}}$ allow to test the rate of cooling during the RGB phase. The method is particularly effective for constraining g_{ae} since in RG cores axions can be efficiently produced via electron bremsstrahlung. The most recent analyses [19–21] have derived comparable constraints. Here we adopt the result of the analysis of the Large Magellanic Cloud in Ref. [22, 23] which provides the most conservative bound $M_{I,\text{TRGB}} = -4.047 \pm 0.045$ mag. In terms of g_{ae} this observable can be written as [19, 24]

$$M_{I,\text{TRGB}}^{\text{theo}} = -4.08 - 0.25 \left(\sqrt{g_{e13}^2 + 0.93} - 0.96 - 0.17g_{e13}^{1.5} \right), \quad (2)$$

which results from an analytic fit to ten evolutionary track points reaching close to the RGB tip obtained from numerical simulations [25], and corresponding to values of g_{e13} up to 9 [19]. The associated theoretical uncertainty is $\sigma^2 = 0.039^2 + (0.046 + 0.012g_{e13})^2$ [19].

- *R-parameter.* After He ignition the RG core expands and its density decreases by two orders of magnitude. The star migrates to the HB and remains supported by He burning in a non-degenerate core. The ratio $R = N_{\text{HB}}/N_{\text{RGB}}$ between the number of stars in in globular clusters in the HB and in the upper portion of the RGB directly measures the duration of He burning in the HB phase. The value $R = 1.39 \pm 0.03$ was obtained in Ref. [26] from the analysis of 39 clusters. The duration of the HB phase can be affected by g_{ae} -related processes both directly and indirectly. If g_{ae} is sufficiently large, axion emission would directly produce extra cooling of the He core. The star self-regulates by slightly contracting, the core temperature increases speeding up the He burning rate. Once the He fuel is exhausted, the star turns into a WD. The indirect effect is related to the growth of the degenerate He core during the RGB phase previously discussed. HB stars would unavoidably inherit a more massive core from the parent RGs, resulting in an increased He burning rate to contrast the larger gravitational pull, and shortening further the duration of the HB phase. Note that the indirect effect of g_{ae} is so important that for $g_{e13} \sim 15$ it would suffice to depopulate almost completely the HB in the Color-Magnitude

Diagram (CMD) ($R \approx 0$). Cooling of HB stars can also proceed via the Primakoff effect $\propto g_{a\gamma}^2$, which is particularly efficient at the typical temperatures and densities of HB cores ($T \sim 10^8$ K, $\rho = 10^4$ g cm $^{-3}$). For sufficiently large values of $g_{a\gamma}$, R can still decrease well below the observed values even when $g_{ae} \approx 0$. Hence an accurate determination of this observable allows to probe the axion coupling to both photons and electrons. In terms of g_{ae} and $g_{a\gamma}$ the R -parameter can be written as [18, 27]

$$R^{\text{theo}} = 7.33Y - 0.095\sqrt{21.86 + 21.08g_{\gamma10}} + 0.02 - 1.61\delta\mathcal{M}_c - 0.005g_{e13}^2, \quad (3)$$

$$\delta\mathcal{M}_c = 0.024 \left(\sqrt{g_{e13}^2 + 1.23^2} - 1.23 - 0.138g_{e13}^{1.5} \right),$$

where $\delta\mathcal{M}_c$ is the change in the He-core mass, and $Y \simeq 0.255 \pm 0.002$ is the primordial He abundance. The relative errors on $\delta\mathcal{M}_c$, which represents the main theoretical uncertainty from astrophysics, and the one on Y , are of the same order. Hence, due to the larger coefficient multiplying Y , the uncertainty from $\delta\mathcal{M}_c$ can be neglected. Similarly to Eq. (2) this expression is derived from an analytic fit to evolutionary track points calculated with stellar evolutionary codes modified to account for axion emission [18, 27], and thus it is quantitatively reliable up to values of g_{ae} not much larger than those corresponding to the last point fitted (for definiteness $g_{e13} \sim 9$). Thus, we will not input into these expressions the much larger XENON1T values $g_{e13} \sim 30$. Rather, very conservatively, we will limit ourselves to estimate the tension between the observed values of $M_{I,\text{TRGB}}$ and R , and the values resulting from Eqs. (2) and (3) when evaluated at $g_{e13} \sim 9$ ($g_{a\gamma} \approx 0$). As regards values of $g_{a\gamma}$ too large to be used in Eq. (3), they can be directly constrained from the lifetime of HB stars which, in the presence of extra cooling, scales as $\sim L_0/(L_0 + L_a)$ with L_0 (L_a) the standard (axion) core luminosity [14]. Hence for $g_{\gamma10} \gtrsim 1$, rather than Eq. (3), we will use

$$R^{\text{theo}} \approx \frac{a^2}{a + bg_{\gamma10}^2}, \quad (4)$$

with $a = (6.26Y - 0.12)$ and $b = 0.41$ [26]. Note that Eq. (4) neglects both direct and indirect effects of g_{ae} on HB and RGB stars, and hence it would also yield conservative limits.

- *White Dwarf luminosity function.* The third observable we consider is the distribution of WDs as a function of their luminosity (WDLF). The WDLF measures the WD cooling efficiency, and thus allows to place strong bounds on new exotic cooling processes, including axion emission (see Ref. [28] for a review). WDs are compact objects whose hydrostatic equilibrium is supported by electron degeneracy pressure, hence axion emission from WDs would dominantly depend on g_{ae} . Here we will use the bound $g_{e13}^{\text{WDLF}} \leq 2.8$ obtained in Ref. [29].

• *Rate of period change of WD variables.* WD variables (WDV) are WDs whose luminosity varies periodically, with a period Π ranging from a few to several minutes. Because the oscillation period depends on the luminosity, a secular change of the period $\dot{\Pi}$ tracks the rate of decrease of the star luminosity. To a very good approximation $\dot{\Pi}/\Pi$ is proportional to the cooling rate \dot{T}/T , hence a measurement of $\dot{\Pi}$ allows to constrain possible sources of extra cooling (see Ref. [30] for a review). Here we consider four WDV: G117-B15A [31], R548 [32], L19-2 [33] (for two pulsation modes), and PG1351+489 [34]. We list in Table I the corresponding measured values of $\dot{\Pi}/\Pi$. Theoretically, the rate of change in the WD pulsating period as a function of g_{e13} can be parametrized as [17]: $\dot{\Pi}_{\text{WD}_i}^{\text{theo}} = a_i + b_i g_{e13}^2$, where a_i and b_i are parameters specific for each WD.

XENON1T vs. Astrophysics. Fig. 1 shows contours of the axion energy-loss rates per unit mass in a temperature vs. density plane, for a pure He plasma. Contour iso-lines for energy-loss due to Compton (dashed blue) and Bremsstrahlung (solid red) processes, which are controlled by g_{ae} , are also shown. For reference, we have fixed $g_{e13} = 4.3$, which corresponds to the RGB bound from M5 [19]. Energy loss rates for different values of g_{ae} can be easily obtained recalling that they scale as g_{ae}^2 . The labelled disks in the figure show the position of the RGB tip and of a typical HB star (of mass $0.8M_\odot$) and a range of WDs with luminosities varying from 5×10^{-4} to $5 \times 10^{-1} L_\odot$ (dashed gray rectangle). The blue disk indicates the temperature/density of a typical WD variable [30]. The location of the Sun is marked with a yellow disk on top of the broken gray line which locates Main Sequence (MS) stars of different masses. Note that since MS stars, including the Sun, are supported by H burning cores, their position with respect to the energy loss iso-lines for the He plasma is approximate, and slightly shifted towards larger rates. The picture shows clearly that the Sun is a relatively faint axion emitter with respect to other stellar objects, so that values $g_{e13} \gtrsim 10$ as required to account for the XENON1T excess would unavoidably turn other stars into bright ‘axion lighthouses’. The RGB would extend to higher luminosities than the ones observed, and the decreased duration of the He burning phase would depopulate the HB, to the point that for smaller clusters with relatively few stars, already for $g_{e13} \sim 15$ we would expect $R \approx 0$. In short, regardless of other details, a value $g_{e13} \sim 30$ would definitely destroy the agreement between stellar evolution models and the observed CMD.

Quantifying the tension. The projections of the XENON1T 90% C.L. best fit region onto the $(g_{ae}, g_{a\gamma})$, $(g_{ae}, g_{an}^{\text{eff}})$ and $(g_{ae}g_{a\gamma}, g_{ae}g_{an}^{\text{eff}})$ planes are given in Fig. 8 of Ref. [1]. Since only g_{ae} and $g_{a\gamma}$ can be responsible for the anomalous XENON1T data below 7 keV, we focus on the best fit region for these two couplings, that

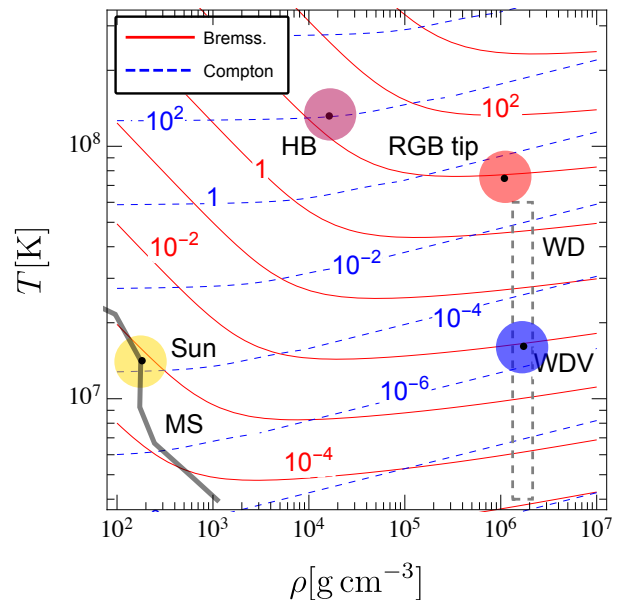


FIG. 1. Contours of the axion energy-loss rates per unit mass, in $\text{erg g}^{-1}\text{s}^{-1}$, for a pure He plasma and $g_{e13} = 4.3$.

corresponds the blue band in Fig. 2. In the figure we also show the 2σ limits on g_{ae} , $g_{a\gamma}$ obtained from each single astrophysical observable, as well as the result of a global fit to the entire set of stellar cooling data. The curve depicting the CAST [35] limit in the $(g_{ae}, g_{a\gamma})$ plane in Ref. [1] was taken from Ref. [36]. We update this bound with the most recent CAST results [37] which, in the $g_{ae} \simeq 0$ limit, and for $m_a \lesssim 20 \text{ meV}$ ($m_a \lesssim 0.7 \text{ eV}$), correspond to $g_{a\gamma} < 0.66 (2.0) \times 10^{-10} \text{ GeV}^{-1}$. These limits are represented in Fig. 2 by the two green lines, in which we have folded in the effects of a non-zero g_{ae} that would increase the production of solar axions and strengthen the bounds. The vertical dashed line is LUX limit [38]. The grey horizontal line at $g_{\gamma 10} = 4.1$ corresponds to the limit from a global fit to solar data, which includes the measured flux of ^8B and ^7Be neutrinos as well as additional data inferred from helioseismology observations [39]. This is about a factor of two stronger than the bound labeled “solar ν ” in the upper panel of Fig. 8 in Ref. [1] which is taken from Ref. [40].² To assess quantitatively the discrepancy between the values of g_{ae} and $g_{a\gamma}$ needed to reproduce the XENON1T excess we proceed as follows: we first extract the allowed ranges from the 90% C.L. region of Ref. [1] not excluded by solar data (the blue area in Fig. 2). This region can be

² For values of the couplings allowed by astrophysics the solar axion luminosity L_a is a negligible fraction of the total luminosity, for example $L_a \approx 1.85 \times 10^{-3} g_{\gamma 10}^2 L_\odot$ for Primakoff emission [40]. Hence, effects on the Sun lifetime are also negligible.

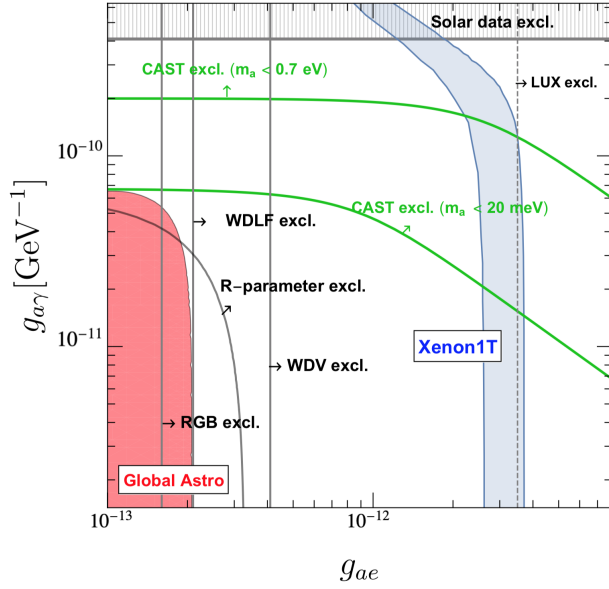


FIG. 2. XENON1T 90% C.L. fit (blue region). 3σ exclusion limit from solar data (grey hatched region). 2σ LUX limit (grey dashed line) and CAST limits for $m_a < 20$ meV and $m_a < 0.7$ eV (green lines). Individual 2σ limits from R -parameter, TRGB, WDLF, WDV (grey lines) and 2σ global bound from astrophysics (red region).

Observable	Measured	Expected	Tension
R -parameter	1.39 ± 0.03	≤ 0.83 ($g_{e13} = 9$)	$19\sigma^*$
$M_{I, \text{TRGB}}^{\text{LMC}}$ [mag]	-4.047 ± 0.045	≤ -4.92 ($g_{e13} = 9$)	$19\sigma^*$
g_{e13}^{WDLF}	≤ 2.8 (3σ)	29.7 ± 4.8	5.6σ
$\dot{\Pi}_{L19-2}^{(113)}$	3.0 ± 0.6	57 ± 16	3.4σ
$\dot{\Pi}_{L19-2}^{(192)}$	3.0 ± 0.6	95 ± 27	3.4σ
$\dot{\Pi}_{\text{PG1351+489}}$	200 ± 90	19620 ± 5730	3.4σ
$\dot{\Pi}_{\text{G117-B15A}}$	4.2 ± 0.7	113 ± 33	3.3σ
$\dot{\Pi}_{\text{R548}}$	3.3 ± 1.1	87 ± 25	3.3σ

TABLE I. Measured values of astrophysic observables and expected ranges, for g_{ae} , $g_{a\gamma}$ falling within the 1σ region of the XENON1T fit ($\bar{g}_{e13} \in [28, 35]$). $\dot{\Pi}_{\text{WDi}}$ are in units of $[10^{-15} \text{ s/s}]$. For R and $M_{I, \text{TRGB}}$ the expected regions and tensions correspond to $g_{e13} = \bar{g}_{e13}(g_{a\gamma} = 0) \geq 9$ (see text).

parametrized by means of an effective coupling [13]

$$\bar{g}_{e13}^4 = g_{e13}^2(g_{e13}^2 + 200g_{\gamma10}^2). \quad (5)$$

The 90% C.L. (68% C.L.) region of XENON1T is then well represented by the range $\bar{g}_{e13} \in [26, 37]$ ($\bar{g}_{e13} \in [28, 35]$). Varying g_{ae} and $g_{a\gamma}$ with the constraint that \bar{g}_{e13} remains within this range, we estimate the range of values for the astrophysical observables implied by the XENON1T data, and we confront them with the measured values. Our results are collected in Table I. For each observable, the tension given in the fourth column

is evaluated by dividing the difference between the value implied by the XENON1T data and the astrophysical determination, by the total uncertainty. Given that the statistical distributions are at best only approximately known, these results are only indicative, and have no rigorous Gaussian meaning. It is apparent that the large g_{ae} required to fit the XENON1T excess are in strong conflict with all the astrophysical observables. The discrepancy is at the level of $\sim 3.4\sigma$ for the WDV's cooling rates (last five rows in the Table), and reaches $\sim 6\sigma$ for the WDLF in the third row. As regards the first two rows, the expected values of R^{theo} and of $M_{I, \text{TRGB}}^{\text{theo}}$ reported in the table are obtained respectively from Eq. (3) and Eq. (2) by setting $g_{e13} = 9$, rather than by inserting the much larger values $g_{e13} \sim 30$ needed to account for the XENON1T data. This is a precautionary procedure that we have adopted to avoid extrapolating Eqs. (2) and (3) to values of g_{ae} for which the quantitative accuracy of these parametrizations cannot be easily assessed. We have then marked with a \star the corresponding tensions. We expect that values of the observables in agreement with the XENON1T solar axion fit would result in much larger tensions. For example, already for $g_{e13} \approx 15$ Eq. (3) would yield $R \approx 0$, corresponding to a complete depopulation of the HB, and 46σ away from observations.

Conclusions. In this work, we have explained why astrophysical observations firmly exclude that solar axions could account for the XENON1T excess. Other explanations based on solar production of new light particles or on modifications of neutrino properties (such as a neutrino magnetic moment) are also prone to severe astrophysical constraints, and as long as the corresponding new physics processes would also occur in RG, HB and WD stellar cores, they can likewise be excluded.³

If it will be eventually found that the tritium background or other systematic effects [42, 43] are not responsible for the excess, other mechanisms involving either absorption or scattering of new particles of non-solar origin off target electrons [44–48], although less compelling than the QCD axion, might still provide viable explanations for the XENON1T data.

Note added. After completing this letter, Refs. [49, 50] appeared claiming that besides the axio-electric effect, also the inverse Primakoff process can contribute to the detection of solar axions by XENON1T. This would relax the best fit region towards lower values of g_{ae} at the cost of increasing $g_{a\gamma}$. This can relax the tension with astrophysical bounds, however, using the results of Ref. [49, 50] we have verified that the discrepancy with the R -parameter remains at least at the level of 8σ .

³ Astrophysical constraints could only be evaded in exotic models in which the couplings strongly depend on the stellar environment, like the core density and temperature, see e.g. [41].

Acknowledgments. We thank Axel Lindner for useful comments. LDL is supported by the Marie Skłodowska-Curie Individual Fellowship grant AXIONRUSH (GA 840791). MF and FM are supported by MINECO grant FPA2016-76005-C2-1-P, Maria de Maetzu program grant MDM-2014-0367 of ICCUB and 2017 SGR 929. EN is supported by the INFN Iniziativa Specifica, Theoretical Astroparticle Physics (TAsP-LNF).

* luca.diluzio@desy.de

† marco.fedele@icc.ub.edu

‡ MGiannotti@barry.edu

§ mescia@ub.edu

¶ enrico.nardi@lnf.infn.it

- [1] E. Aprile *et al.* (XENON), (2020), [arXiv:2006.09721 \[hep-ex\]](#).
- [2] J. Redondo, *JCAP* **12**, 008 (2013), [arXiv:1310.0823 \[hep-ph\]](#).
- [3] H. Primakoff, *Phys. Rev.* **81**, 899 (1951).
- [4] S. Moriyama, *Phys. Rev. Lett.* **75**, 3222 (1995), [arXiv:hep-ph/9504318 \[hep-ph\]](#).
- [5] R. D. Peccei and H. R. Quinn, *Phys. Rev. Lett.* **38**, 1440 (1977).
- [6] R. D. Peccei and H. R. Quinn, *Phys. Rev.* **D16**, 1791 (1977).
- [7] S. Weinberg, *Phys. Rev. Lett.* **40**, 223 (1978).
- [8] F. Wilczek, *Phys. Rev. Lett.* **40**, 279 (1978).
- [9] L. Di Luzio, F. Mescia, and E. Nardi, *Phys. Rev. Lett.* **118**, 031801 (2017), [arXiv:1610.07593 \[hep-ph\]](#).
- [10] L. Di Luzio, F. Mescia, and E. Nardi, *Phys. Rev. D* **96**, 075003 (2017), [arXiv:1705.05370 \[hep-ph\]](#).
- [11] L. Di Luzio, F. Mescia, E. Nardi, P. Panci, and R. Ziegler, *Phys. Rev. Lett.* **120**, 261803 (2018), [arXiv:1712.04940 \[hep-ph\]](#).
- [12] F. Björkeröth, L. Di Luzio, F. Mescia, E. Nardi, P. Panci, and R. Ziegler, *Phys. Rev. D* **101**, 035027 (2020), [arXiv:1907.06575 \[hep-ph\]](#).
- [13] L. Di Luzio, M. Giannotti, E. Nardi, and L. Visinelli, (2020), [arXiv:2003.01100 \[hep-ph\]](#).
- [14] G. Raffelt, *Stars as laboratories for fundamental physics: The astrophysics of neutrinos, axions, and other weakly interacting particles* (1996).
- [15] S. Hoof, F. Kahlhoefer, P. Scott, C. Weniger, and M. White, *JHEP* **03**, 191 (2019), [Erratum: *JHEP* **11**, 099 (2019)], [arXiv:1810.07192 \[hep-ph\]](#).
- [16] P. Di Vecchia, M. Giannotti, M. Lattanzi, and A. Lindner, *PoS Confinement2018*, 034 (2019), [arXiv:1902.06567 \[hep-ph\]](#).
- [17] M. Giannotti, I. G. Irastorza, J. Redondo, A. Ringwald, and K. Saikawa, *JCAP* **10**, 010 (2017), [arXiv:1708.02111 \[hep-ph\]](#).
- [18] M. Giannotti, I. Irastorza, J. Redondo, and A. Ringwald, *JCAP* **05**, 057 (2016), [arXiv:1512.08108 \[astro-ph.HE\]](#).
- [19] N. Viaux, M. Catelan, P. B. Stetson, G. Raffelt, J. Redondo, A. A. R. Valcarce, and A. Weiss, *Phys. Rev. Lett.* **111**, 231301 (2013), [arXiv:1311.1669 \[astro-ph.SR\]](#).
- [20] O. Straniero, I. Dominguez, M. Giannotti, and A. Mirizzi, in *13th Patras Workshop on Axions, WIMPs and WISPs* (2018) pp. 172–176, [arXiv:1802.10357 \[astro-ph.SR\]](#).
- [21] S. A. Díaz, K.-P. Schröder, K. Zuber, D. Jack, and E. E. B. Barrios, (2019), [arXiv:1910.10568 \[astro-ph.SR\]](#).
- [22] W. L. Freedman *et al.*, (2019), [10.3847/1538-4357/ab2f73](#), [arXiv:1907.05922 \[astro-ph.CO\]](#).
- [23] W. L. Freedman, B. F. Madore, T. Hoyt, I. S. Jang, R. Beaton, M. G. Lee, A. Monson, J. Neeley, and J. Rich, (2020), [10.3847/1538-4357/ab7339](#), [arXiv:2002.01550 \[astro-ph.GA\]](#).
- [24] F. Capozzi and G. Raffelt, (2020), [arXiv:2007.03694 \[astro-ph.SR\]](#).
- [25] N. Viaux, M. Catelan, P. B. Stetson, G. Raffelt, J. Redondo, A. A. R. Valcarce, and A. Weiss, *Astron. Astrophys.* **558**, A12 (2013), [arXiv:1308.4627 \[astro-ph.SR\]](#).
- [26] A. Ayala, I. Domínguez, M. Giannotti, A. Mirizzi, and O. Straniero, *Phys. Rev. Lett.* **113**, 191302 (2014), [arXiv:1406.6053 \[astro-ph.SR\]](#).
- [27] O. Straniero, A. Ayala, M. Giannotti, A. Mirizzi, and I. Dominguez, in *11th Patras Workshop on Axions, WIMPs and WISPs* (2015) pp. 77–81.
- [28] J. Isern, in *IAU Symposium 357: White Dwarfs as probes of fundamental physics and tracers of planetary, stellar & galactic evolution* (2020) [arXiv:2002.08069 \[astro-ph.SR\]](#).
- [29] M. M. Miller Bertolami, B. E. Melendez, L. G. Althaus, and J. Isern, *JCAP* **10**, 069 (2014), [arXiv:1406.7712 \[hep-ph\]](#).
- [30] A. H. Córscico, L. G. Althaus, M. M. Miller Bertolami, and S. Kepler, *Astron. Astrophys. Rev.* **27**, 7 (2019), [arXiv:1907.00115 \[astro-ph.SR\]](#).
- [31] A. H. Corsico, L. G. Althaus, M. M. Bertolami, A. D. Romero, E. Garcia-Berro, J. Isern, and S. Kepler, *Mon. Not. Roy. Astron. Soc.* **424**, 2792 (2012), [arXiv:1205.6180 \[astro-ph.SR\]](#).
- [32] A. Corsico, L. Althaus, A. Romero, A. Mukadam, E. Garcia-Berro, J. Isern, S. Kepler, and M. Corti, *JCAP* **12**, 010 (2012), [arXiv:1211.3389 \[astro-ph.SR\]](#).
- [33] A. H. Córscico, A. D. Romero, L. G. Althaus, E. García-Berro, J. Isern, S. Kepler, M. M. Miller Bertolami, D. J. Sullivan, and P. Chote, *JCAP* **07**, 036 (2016), [arXiv:1605.06458 \[astro-ph.SR\]](#).
- [34] T. Battich, A. H. Córscico, L. G. Althaus, M. M. Miller Bertolami, and M. Bertolami, *JCAP* **08**, 062 (2016), [arXiv:1605.07668 \[astro-ph.SR\]](#).
- [35] S. Andriamonje *et al.* (CAST), *JCAP* **12**, 002 (2009), [arXiv:0906.4488 \[hep-ex\]](#).
- [36] K. Barth *et al.*, *JCAP* **05**, 010 (2013), [arXiv:1302.6283 \[astro-ph.SR\]](#).
- [37] V. Anastassopoulos *et al.* (CAST), *Nature Phys.* **13**, 584 (2017), [arXiv:1705.02290 \[hep-ex\]](#).
- [38] D. Akerib *et al.* (LUX), *Phys. Rev. Lett.* **118**, 261301 (2017), [arXiv:1704.02297 \[astro-ph.CO\]](#).
- [39] N. Vinyoles, A. Serenelli, F. L. Villante, S. Basu, J. Redondo, and J. Isern, *JCAP* **10**, 015 (2015), [arXiv:1501.01639 \[astro-ph.SR\]](#).
- [40] P. Gondolo and G. G. Raffelt, *Phys. Rev. D* **79**, 107301 (2009), [arXiv:0807.2926 \[astro-ph\]](#).
- [41] J. Redondo, *Can the PVLAS particle be compatible with the astrophysical bounds?*, Ph.D. thesis, Barcelona, Autònoma U. (2007), [arXiv:0807.4329 \[hep-ph\]](#).
- [42] C. Dessert, J. W. Foster, Y. Kahn, and B. R. Safdi, (2020), [arXiv:2006.16220 \[hep-ph\]](#).
- [43] M. Szydagis, C. Levy, G. Blockinger, A. Kamaha, N. Parveen, and G. Rischbieter, (2020), [arXiv:2007.00528 \[hep-ex\]](#).

- [44] F. Takahashi, M. Yamada, and W. Yin, (2020), [arXiv:2006.10035 \[hep-ph\]](#).
- [45] K. Kannike, M. Raidal, H. Veermäe, A. Strumia, and D. Teresi, (2020), [arXiv:2006.10735 \[hep-ph\]](#).
- [46] G. Alonso-Álvarez, F. Ertas, J. Jaeckel, F. Kahlhoefer, and L. Thormaehlen, (2020), [arXiv:2006.11243 \[hep-ph\]](#).
- [47] C. Boehm, D. G. Cerdeno, M. Fairbairn, P. A. Machado, and A. C. Vincent, (2020), [arXiv:2006.11250 \[hep-ph\]](#).
- [48] B. Fornal, P. Sandick, J. Shu, M. Su, and Y. Zhao, (2020), [arXiv:2006.11264 \[hep-ph\]](#).
- [49] C. Gao, J. Liu, L.-T. Wang, X.-P. Wang, W. Xue, and Y.-M. Zhong, (2020), [arXiv:2006.14598 \[hep-ph\]](#).
- [50] J. B. Dent, B. Dutta, J. L. Newstead, and A. Thompson, (2020), [arXiv:2006.15118 \[hep-ph\]](#).